Available online at www.sciencedirect.com
ScienceDirect
Ad Hoc Networks 00 (2023) 1–18
Ad Hoc Networks

Hybrid Fusion of Pietra-Ricci Index Detector Information for Cooperative Spectrum Sensing

Dayan Adionel Guimarães

National Institute of Telecommunications - Inatel, Av. João de Camargo, 510, 37540-000, Santa Rita do Sapucaí, MG, Brazil.

Abstract

The Pietra-Ricci index detector (PRIDe) has been recently proposed as one of the simplest techniques for data-fusion cooperative spectrum sensing (CSS), attaining robustness against time-varying signal and noise levels, constant false alarm rate, and high performance. This paper proposes a hybrid sensing information fusion scheme for cluster-based CSS, in which the PRIDe is applied to data-fusion at the cluster heads (CHs), in combination with decision-fusion of CHs' decisions at the fusion center. A modified version of the *k*-means clustering algorithm is used to form the clusters, where a CH is defined as the cluster member closest to the cluster's centroid. Theoretical and computer-simulation results trade the spectrum sensing performance against the energy per bit effectively transmitted during the data communication interval, unveiling that, contrary to the common thought, cluster-based CSS may not provide energy savings compared to CSS without clustering. Moreover, it is demonstrated that the performance rank of the well-known decision-fusion rules AND, OR and MAJ is strongly affected by the distance between the primary network transmitter and the secondary users, as well as by the path-loss exponent of the sensing channel.

Keywords: Cluster-based cooperative spectrum sensing, cognitive radio, data-fusion cooperative spectrum sensing, decision-fusion cooperative spectrum sensing, *k*-means clustering, Pietra-Ricci index detector (PRIDe).

1. Introduction

The growth of wireless communication systems in recent years has led to a scarcity of the radio-frequency (RF) spectrum. This is owed mainly to the adoption of a fixed spectrum allocation policy, which grants exclusive rights to a primary user (PU) network. Nonetheless, in some regions and at certain times, the allocated bands may be underutilized, resulting in inefficient spectrum usage.

The massive deployment of the Internet of Things (IoT) and the fifth generation (5G) of wireless communication networks is expected to worsen the RF spectrum shortage, as the large expected number of terminals will demand even higher bandwidths, which is also a trend regarding beyond-5G networks. To alleviate this shortage, a cognitive radio (CR) network can be adopted to explore unoccupied frequency bands using a dynamic spectrum access policy, with cognitive secondary user (SU) terminals opportunistically using vacant bands [1, 2].

Spectrum sensing [3, 4, 2, 5], with or without the aid of an RF spectrum occupancy database [6], is used by the secondary network to detect spectral holes. However, it is known that independent spectrum sensing by each SU is prone to performance degradation [2], meaning that cooperative spectrum sensing (CSS) is the preferred solution. CSS involves multiple SUs co-participating in the sensing process to improve the accuracy of channel occupation state

Email address: dayan@inatel.br ()
URL: https://www.inatel.br/docentes/dayan/ ()

decisions. The most common form of CSS is the centralized approach, in which the sensing information gathered by the SUs are transmitted to the fusion center (FC) of the secondary network, where the decision upon the state of the sensed channel is made.

When centralized CSS takes place, there are often two alternatives for combining the sensing information at the FC: i) In data-fusion CSS (sometimes called sample-fusion CSS), the received signal samples collected by the SUs, or any soft-information derived from these samples are forwarded to the FC, where a test statistic is formed and compared with a decision threshold to yield the global decision on the occupation state of the sensed band. ii) In decision-fusion CSS, a test statistic is formed in each SU, allowing for a local spectrum occupancy decision. The SUs' decisions are subsequently forwarded to the FC, where a hard-decision combining rule is applied to the local decisions to yield the global decision.

The well-known hard-decision combining approach is the κ-out-of-c rule, in which the FC decides in favor of the presence of the primary signal if κ or more SUs decide in the same manner. Common special cases of this rule are the so-called OR (for $\kappa = 1$), AND (for $\kappa = c$), and majority (MAJ) voting (for $\kappa = \lfloor c/2 + 1 \rfloor$, where $\lfloor x \rfloor$ is the greatest integer less than or equal to x). Although there is no general expected outcome regarding the influence of the hard-decision combining approach chosen, it significantly depends on the spectrum sensing performances of the SUs. The MAJ rule normally wins when these performances are the same, with the performance rank of OR, AND and MAJ varying considerably if the performances are different from each other.

In either data-fusion or decision-fusion, the global decision made at the FC is broadcasted to the SUs, which will subsequently compete for the band, if it is vacant, using any appropriate multiple access technique.

Decision-fusion is known to deliver worse spectrum sensing performances in comparison to data-fusion, and larger computational complexity of the SUs due to the need of computing local test statistics. However, decision-fusion CSS is often referred as capable of potentially increasing the secondary network throughput, while reducing its energy consumption due to the smaller amount of data that is reported to the FC in comparison with data-fusion CSS. Hence, the choice between data-fusion and decision-fusion CSS seems to rely on a trade-off analysis involving spectrum sensing performance, energy consumption and data throughput.

The cluster-based CSS [7] strategy lies in-between pure data-fusion and pure decision-fusion CSS. In a cluster-based CSS system, nodes are grouped into clusters, with cluster members sending their sensing information to cluster heads (CHs), and CHs sending the received sensing information data (with or without its own sensing data) to the central node for fusion. Cluster-based CSS can potentially provide energy savings compared to CSS without clustering, owed mainly to the reduction in the amount of data transmission and processing overhead. At the same time, it aims at improving the performance relative to pure decision-fusion CSS.

Among the variety of detectors designed so far for spectrum sensing, the Pietra-Ricci index detector (PRIDe) [8] has been recently proposed as one of the simplest techniques for centralized data-fusion CSS, attaining robustness against time-varying signal and noise levels, constant false alarm rate, and high detection capability. In this paper, a cluster-based hybrid-fusion CSS approach is proposed, in which clusters of SUs are formed and the PRIDe is used as the test statistic generated at the CHs using data-fusion CSS. The decisions made by the CHs are then are forwarded to the FC, applying a decision-fusion CSS strategy. The hybrid fusion aims at attaining the attractive attributes of decision-fusion and data-fusion CSS, namely: smaller energy consumption and potential higher throughput of the former, combined with better performance of the latter.

1.1. Related research

Several test statistics have been developed for spectrum sensing, many of them relying on processing the elements of the sample covariance matrix (SCM) of the received signal [9, 10, 11, 12, 13, 14, 8]. Among the SCM-based test statistics, it can be mentioned the Hadamard ratio (HR) detector [9], the arithmetic to geometric mean (AGM) detector [10], the volume-based detectors (VD) [11], the maximum-minimum eigenvalue detector (MMED), the eigenvalue-based generalized likelihood ratio test (GLRT) [12], the Gini index detector (GID) [13], the Gerschgorin radii and centers ratio (GRCR) [14], and the already-mentioned Pietra-Ricci index detector (PRIDe) [8].

The computational burden associated to the test statistics for the detectors HR and VD depends mainly on calculating the determinant of the SCM (in the case of HR) or another matrix derived from the SCM (in the case of VD). Detectors such as the AGM, the MMED, and the eigenvalue-based GLRT rely on computing the eigenvalues of the SCM to construct the test statistics. In contrast, the GID, GRCR and PRIDe directly operate on the elements of the SCM to build their test statistics without utilizing eigenvalues, determinants or other equally complex operations.

The detectors HR, VD, AGM, MMED, GLRT, GID, GRCR and PRIDe are considered blind, in the sense that they do not rely on information about the noise variance, nor about the characteristics of the primary signal. The GID, GRCR and PRIDe detectors are noteworthy because they have lower computational complexity compared to the others, being also robust against changes in the powers of the received signal and noise. Among these detectors, the PRIDe is the least complex [8].

In regard to the research efforts on energy-efficient CSS techniques, several authors have proposed methods to reduce energy expenditure, for example adopting optimization strategies at some stage of the sensing process [15, 16, 17]. Techniques to reduce the number of radios that transmit during the SUs information exchange stage have been also proposed, for instance in [18, 19].

A survey of energy-efficient CSS schemes is presented in [7], where the cluster-based approach is defined as the one considering that cluster members report their local decisions to the corresponding CH. The role of the CHs is to either forward the received cluster members' decisions to the FC, or to make a decision at the cluster level, subsequently reporting it to the FC, where the final decision takes place under a hard-decision combining rule.

In [20], it is proposed a hybrid cluster-based CSS in which clusters are defined according to sensing reliability and energy efficiency, with the term 'hybrid' referring to the use of these two metrics. The SUs apply energy detection and transmit their decisions to the secondary network's base-station, where a majority voting decision rule is applied. The CHs are meant to relay data traffic from the cluster members to the base-station, also acting as sensing nodes.

An iterative algorithm is proposed in [21] to determine joint optimal sensing time, data transmission time, and the number of SUs that maximize energy efficiency of a cluster-based CSS scheme. The cluster members independently detect the presence of the PU signal, forwarding their decisions to the CH, which combines the observations using the κ-out-of-c rule. The CH decides either to transmit data if the sensed band is unoccupied, or to sleep if the PU signal is declared present.

The cluster-based CSS scheme considered in [22] also adopts the approach of transmitting the SUs decisions to the CHs, which forward them to the FC, where the κ-out-of-c rule is applied. The individual SUs decisions are made via energy detection. The authors propose multiple reporting channels to enhance the spectrum sensing performance and reduce the reporting time delay of the CHs.

An optimal linear weighted CSS for cluster-based topology is proposed in [23]. The cluster members apply energy detection and forward the captured signal energies to the CH, where they are combined under weights determined according to the signal-to-noise ratio (SNR) and the historical sensing accuracy. The decisions made by the CHs are forwarded to the FC, where the OR rule is applied.

The sensing throughput trade-off problem is addressed in [24], where a cluster-based CSS is also adopted. Energy detection is performed by the cluster members, which report their decisions to the head user (equivalent to the CH). Each head user then applies the κ-out-of-c rule and forwards the decision to the FC, where the head users' decisions are combined using the OR rule.

From the research reported, it can be seen that most of the proposed cluster-based CSS approaches consider energy detection at the SU level, performing intermediate hard-decision combining at the CH and a final hard-decision combining at the FC. The single identified reference that makes soft-combining at the CH level, yet using energy detection, is [23]. However, recall that the energy detector is not blind, since it needs to know the noise variance to proper establish the decision threshold, and it may suffer from large performance loss due to noise uncertainty [25]. On the other hand, many proposals adopt unrealistic assumptions for analyzing the network performance, resulting in equally unrealistic analyses and conclusions. Examples are the adoption of the same SNR and the same spectrum sensing performance for all SUs [26], in some cases neglecting the influence of relevant propagation phenomena of the sensing channel [27, 28]. Motivated by these facts, the framework proposed herein adopts a realistic system model in combination with a state-of-the-art blind detector, aiming at forming a hybrid cluster-based CSS from which it is possible to draw solid conclusions regarding the trade-off between spectrum sensing performance and energy savings in the secondary network.

1.2. Contribution and structure of the article

This paper proposes and analyzes a cluster-based CSS scheme in which soft-decision-fusion at the CHs is combined with hard-decision-fusion at the FC, so the given name 'hybrid fusion'. Differently from the common use of energy detection, the soft-decision-fusion part of the hybrid scheme applies data-fusion CSS at the clusters level, by

forming PRIDe test statistics at the CHs. The decisions made at the CHs are forwarded to the FC, where the final decision is reached by means of the κ-out-of-c rule. A modified version of the k-means clustering algorithm is used to form the clusters, under the restriction that the minimum number of cluster members is 2. This restriction is necessary for the proper operation of the PRIDe detector (or any other SCM-based detector), since it is subsumed that the order of the SCM is at least 2. Numerical results trade the spectrum sensing performance against the energy per bit effectively transmitted during the data communication phase. As a byproduct, it is also provided a comprehensive Matlab code [29] for simulating the proposed hybrid fusion scheme in a variety of circumstances and system parametrization. In summary, the main contributions of this work are:

- A hybrid information fusion for cluster-based CSS, in which data-fusion at the cluster level, using the PRIDe, is combined with decision-fusion CSS at the FC level.
- A modified version of the k-means clustering algorithm that guarantees that no cluster has less than 2 members, making it feasible the use of the covariance-matrix-based PRIDe test statistic in the data-fusion part.
- A practical-appealing system model that adopts realistic clustering, distance-dependent path-loss, sensing channel fading with variable line-of-sight condition, and variable signal and noise levels across the SUs.
- A plenty of numerical results, including theoretical ones, to support the conclusions of the work.
- A fully-commented comprehensive Matlab simulation code [29] capable of supporting a complete system analysis under a variety of circumstances and system parameters.

The remainder sections of the article are organized as follows. Section 2 presents the clustering strategy adopted in the hybrid fusion scheme. The cooperative spectrum sensing model is described in Section 3, along with the PRIDe test statistic. Section 4 addresses the model for assessing the energy consumption of the secondary network. Numerical results are presented and commented in Section 5. The conclusions are given in Section 6.

2. Clustering model

It is assumed that the SUs positions, which are determined by two-dimensional coordinates (x, y), are randomly distributed throughout the primary network coverage area, which is assumed to be circular with radius r.

The necessary information to the clustering process, which is determined in the deployment phase of the hybrid CSS scheme, is the maximum number of clusters, $c_{\max}$, and the total number of SUs, m_{T}. The total number of SUs is divided into $c \leq c_{\max}$ clusters, each cluster containing $m_j \geq 2$ members, for $j = 1, \ldots, c$. The clusters are formed according to a modified version of the k-means clustering algorithm [30, 31]. Since the PRIDe subsumes that the order of the SCM is at least 2, the modification in the k-means algorithm guarantees that each cluster contains at least 2 members, which is made by executing the algorithm firstly with $k = c_{\max}$ and testing if any cluster has a single member. If true, the algorithm is repeated for $k \leftarrow k - 1$, until there is no more clusters having a single member. The final number of clusters is $c = k$, with $c \leq c_{\max}$.

The unmodified k-means clustering algorithm aims at grouping similar data points together into clusters. It starts by randomly selecting k points from the set to serve as the initial cluster centroids. A centroid is the central point in a cluster of points or, equivalently, it is the average of the coordinates of the cluster's members. The k-means clustering algorithm finds the best k centroids to divide the data into k clusters such that the sum of the squared distances between each cluster component and its nearest centroid is minimized. Each point is assigned to the closest centroid. Next, the algorithm updates the position of the centroids to be the average of all the points assigned to that centroid. This process of reassigning points to centroids and updating the centroids is repeated until the centroids no longer change significantly. In the end, each point is assigned to a cluster based on its closest centroid, resulting in k clusters.

Figure 1 shows a random realization of the k-means clustering process for $m_{\mathrm{T}} = 15$ and $c_{\max} = c = 3$. In Matlab, which has been used to plot this figure, the k-means clustering algorithm is performed by the function `kmeans` [32]. The SUs, the PU transmitter ($\mathrm{PU_{tx}}$), the FC - which is also the base-station (BS) of the secondary network, the CHs, and the cluster centroids are also shown. Are also shown: the Voronoi regions' frontiers that separate the clusters, and the perimeter of the circular coverage area where the SUs are uniformly distributed. The CHs are defined as the SUs located closest to the clusters' centroids. In this exemplifying scenario, the number of SUs in each cluster are $m_1 = 6$,

$m_2 = 3$, and $m_3 = 6$. The area radius is normalized to $r = 1$ m, and in this case the PU_{tx} is located at the coordinates $(r, r) = (1, 1)$ m. The FC coordinates are $(0, 0)$, meaning that it is positioned at the center of the coverage area of the secondary network.

In Figure 1, the node PU_{tx} is the transmitter of the primary network. Three types of nodes belonging to the secondary network can be identified in this figure: The SUs that perform spectrum sensing, the SUs that are designated cluster heads (CHs) used as intermediate fusion centers of the sensing information transmitted by the clusters' SUs, additionally acting as spectrum sensors, and a node that works as the fusion center (FC) of the cluster heads' decisions. If no clustering is adopted, there are two types of nodes in the secondary network: The SUs that perform spectrum sensing, and the central node that acts as the fusion center of the signal samples collected by the SUs.

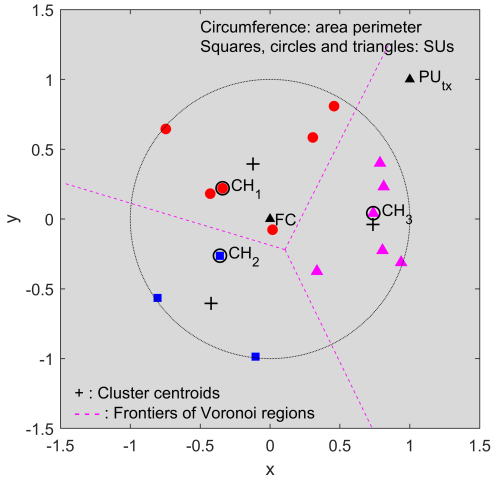

Figure 1. Clustering via the modified k-means algorithm.

It is worth highlighting that if $c_{\max} > m_{\text{T}}/2$, then $c < c_{\max}$ with probability 1, since m_{T}/c must be greater than, or equal to 2. For example, for $m_{\text{T}} = 16$ and $c_{\max} = 9$, the number of clusters resulting from the modified k-means algorithm is at most $c = 8$, which corresponds to 2 members per cluster. Moreover, if $c_{\max} > m_{\text{T}}/2$, the execution time of the algorithm increases, since it will be repeated for successively smaller k, departing from $c_{\max}$, up to $m_{\text{T}}/2$. After that, it is likely that the algorithm repeats for even smaller values of k, until there is no cluster with less than 2 members. The probability that the algorithm is repeated for $k < m_{\text{T}}/2$ increases for larger values of m_{T}.

3. Spectrum sensing model

This section describes the overall CSS model adopted in this article, starting with the signal, noise and channel models, followed by the presentation of the PRIDe test statistic, and ending with the model for performance analysis.

3.1. Signal, noise and channel models

In the jth cluster, for $j = 1, \ldots, c$, the CSS uses m_j SUs, each one gathering n samples of the PU signal during the sensing interval. The samples collected by the SUs of a cluster, including the CH, are aggregated at the jth CH to form the matrix $\mathbf{Y}_j \in \mathbb{C}^{m_j \times n}$ given by

$$\mathbf{Y}_j = \mathbf{h}_j \mathbf{x}^{\text{T}} + \mathbf{V}_j, \tag{1}$$

where the vector $\mathbf{x} \in \mathbb{C}^{n \times 1}$ contains the PU signal samples, which are zero-mean complex Gaussian random variables whose variance is determined according to the average SNR across the SUs.

The channel vector $\mathbf{h}_j \in \mathbb{C}^{m_j \times 1}$ is formed by elements $h_{i,j}$, $i = 1, \ldots, m_j$, representing the channel gains between the PU transmitter and the ith SU of the jth cluster. These gains are constant during the sensing interval and independent

and identically distributed (i.i.d.) over the sensing rounds. The channel vector is given by $\mathbf{h}_j = \mathbf{G}_j\mathbf{a}_j$, where $\mathbf{G}_j$ is a gain matrix to be defined ahead, and $\mathbf{a}_j \in \mathbb{C}^{m_j\times 1}$ is a vector formed by complex-Gaussian random variates $a_{i,j} \sim \mathbb{C}\mathcal{N}[\sqrt{K_{i,j}/(2K_{i,j}+2)}, 1/(K_{i,j}+1)]$, where $K_{i,j} = 10^{K_{i,j}^{(\mathrm{dB})}/10}$, with $K_{i,j}^{(\mathrm{dB})} = 10\log_{10}(K_{i,j})$ being the Rice factor, in dB, of the channel between the PU and the ith SU of the jth cluster. From [33], it can be found that $K_{i,j} \sim \mathcal{N}[\mu_K, \sigma_K]$ is an environment-dependent Gaussian random variable, with mean μ_K and standard deviation σ_K, both in dB, determined according to the propagation characteristics of the area. An urban area is considered herein, for which $\mu_K = 1.88$ dB and $\sigma_K = 4.13$ dB [33].

Unequal and time-varying received signal power levels across the SUs occur due to the different distances between the PU transmitter and the SUs, and due to the variation of these distances across different sensing rounds due to SUs' motion. This is modeled by setting the diagonal gain matrix $\mathbf{G}_j \in \mathbb{R}^{m_j\times m_j}$ as $\mathbf{G}_j = \mathrm{diag}(\sqrt{\mathbf{p}_j/P_{\mathrm{txPU}}})$, where $\mathbf{p}_j = [P_{\mathrm{rxSU}1,j}\, P_{\mathrm{rxSU}2,j}\, \ldots\, P_{\mathrm{rxSU}m_j,j}]^{\mathrm{T}}$ is the vector with the received PU signal powers across the m_j SUs of the jth cluster, with $[\cdot]^{\mathrm{T}}$ denoting transposition, P_{txPU} is the transmitted PU signal power, and $\mathrm{diag}(\cdot)$ returns a diagonal matrix whose diagonal is formed by the vector in the argument.

The PU signal power received by the ith SU of the jth cluster, for $i = 1, \ldots, m_j$, is determined via the log-distance path-loss prediction model [34, p. 202], yielding

$$P_{\mathrm{rxSU}i,j} = P_{\mathrm{txPU}}\left(\frac{d_0}{d_{\mathrm{PU}_{i,j}}}\right)^{\eta}, \tag{2}$$

where d_0 is a reference distance in the far-field region of the PU transmit antenna, $d_{\mathrm{PU}_{i,j}}$ is the distance from the PU transmitter to the ith SU of the jth cluster, and η is the environment-dependent dimensionless path-loss exponent. Larger values of η means larger signal attenuation.

The variability of thermal noise is also assumed in the present model. Across a large area, this variability can be significant and depends on multiple factors, including temperature, physical properties of the receiver components, and environmental conditions such as electromagnetic interference, atmospheric noise, and radio-frequency interference that are added to the receiver noise as if they were thermal noise. Herein, the nonuniform and time-varying noise level is modeled as follows: The elements in the ith row of the matrix $\mathbf{V}_j \in \mathbb{C}^{m_j\times n}$ in (1) are independent, with respect to i and j, Gaussian random variables with zero mean and variance

$$\sigma_i^2 = (1+\rho u_i)\bar{\sigma}^2, \tag{3}$$

where u_i is the realization of a uniform random variable U_i in the interval $[-1, 1]$, that is, $U_i \sim \mathcal{U}[-1, 1]$, $\bar{\sigma}^2$ is the noise variance averaged across all SUs, and $0 \le \rho < 1$, which is a predefined parameter of the model, is the fractional variation of the noise power about $\bar{\sigma}^2$.

The signal-to-noise ratio averaged across the SUs of the jth cluster is denoted as SNR_j. It is also a random variable, since it depends on σ_i^2 and on the distances $d_{\mathrm{PU}_{i,j}}$, which vary according to the SUs' positions. In light of (2) and (3), a realization of SNR_j is given by

$$\mathrm{SNR}_j = \frac{1}{m_j}\sum_{i=1}^{m_j}\frac{P_{\mathrm{txPU}}\left(d_0/d_{\mathrm{PU}_{i,j}}\right)^{\eta}}{(1+\rho u_i)\bar{\sigma}^2}. \tag{4}$$

Thus, the global average SNR across all SUs, which is also a predefined parameter of the model, is given by

$$\mathrm{SNR} = \frac{1}{c}\sum_{j=1}^{c}\mathbb{E}[\mathrm{SNR}_j], \tag{5}$$

where $\mathbb{E}[\mathrm{SNR}_j]$ is the expected value of SNR_j.

To implement such a variable noise level model for computer simulation purposes, firstly it has to be calculated the expectation of the uncalibrated SNR'_j, which is defined for an uncalibrated average noise variance $\bar{\sigma}^2 = 1$, and for a given realization of the SUs' locations. This expectation is derived in the **Appendix A**. For $\rho = 0$, it is given by

$$\mathbb{E}[\mathrm{SNR}'_j] = \frac{1}{m_j}\sum_{i=1}^{m_j}P_{\mathrm{rxSU}i,j} \tag{6}$$

and for $0 < \rho < 1$ it is given by

$$\mathbb{E}[\mathrm{SNR}'_j] = \ln\left(\frac{1+\rho}{1-\rho}\right)\frac{1}{2\rho m_j}\sum_{i=1}^{m_j} P_{\mathrm{rxSU}\,i,j}. \tag{7}$$

Having computed $\mathbb{E}[\mathrm{SNR}'_j]$, a global uncalibrated SNR' is calculated via (5), that is, $\mathrm{SNR}' = \frac{1}{c}\sum_{j=1}^{c}\mathbb{E}[\mathrm{SNR}'_j]$. Then, the calibrated value of the average noise variance is given by

$$\bar{\sigma}^2 = \frac{\mathrm{SNR}'}{\mathrm{SNR}}. \tag{8}$$

Finally, this $\bar{\sigma}^2$ is plugged into (3), along with a realization of U_i, to yield σ_i^2, which is the variance of the noise samples in the ith row of the matrix $\mathbf{V}_j$ for all j. New values of the set $\{\sigma_i^2\}$ are computed in each sensing round, conferring the desired time-varying character to the noise level.

The procedure just described, which can be easily identified in the source code [29], is repeated whenever a new clustering is performed from a new realization of the SUs' locations.

At this point of the spectrum sensing process, the matrix $\mathbf{Y}_j$ defined in (1) is computed by the jth CH. Under the hypothesis $\mathcal{H}_0$, the primary signal is absent in the sensed band, yielding $\mathbf{Y}_j = \mathbf{V}_j$. Under the hypothesis $\mathcal{H}_1$, it follows that $\mathbf{Y}_j = \mathbf{h}_j\mathbf{x}^{\mathrm{T}} + \mathbf{V}_j$.

Given $\mathbf{Y}_j$, the SCM of order m_j is subsequently formed at the jth CH, according to

$$\mathbf{R}_j = \frac{1}{n}\mathbf{Y}_j\mathbf{Y}_j^{\dagger}, \tag{9}$$

where † denotes complex conjugate and transpose.

It is worth mentioning that if $c_{\max} = 1 = c$, the single matrix $\mathbf{Y}_j = \mathbf{Y}_1$ and, consequently, the single SCM $\mathbf{R}_j = \mathbf{R}_1$ are computed at the FC, since there is no CH.

3.2. PRIDe test statistic

Given $\mathbf{R}_1$ at the FC when $c_{\max} = 1$, or $\mathbf{R}_j$ at the jth CH when $c_{\max} > 1$, the PRIDe test statistic is computed as follows. Let $r_{j,z,k}$ denote the element in the zth row and kth column of $\mathbf{R}_j$, for $j = 1, \ldots, c$ and $z, k = 1, \ldots, m_j$, and let the average of $r_{j,z,k}$ over z and k be

$$\bar{r}_j = \frac{1}{m_j^2}\sum_{z=1}^{m_j}\sum_{k=1}^{m_j} r_{j,z,k}. \tag{10}$$

The PRIDe test statistic originally proposed in [8], computed by the jth CH or by the FC, using a slightly-modified notation adapted to the present cluster-based approach, is

$$T_{\mathrm{PRIDe}_j} = \frac{\sum_{z=1}^{m_j}\sum_{k=1}^{m_j}\left|r_{j,z,k}\right|}{\sum_{z=1}^{m_j}\sum_{k=1}^{m_j}\left|r_{j,z,k} - \bar{r}_j\right|}. \tag{11}$$

The decision upon the occupation state of the sensed band is made at the jth CH ($j = 1, \ldots, c$), or at the FC ($j = 1$), by comparing T_{PRIDe_j} with a decision threshold λ_j. If $T_{\mathrm{PRIDe}_j} > \lambda_j$, the decision is made in favor of the hypothesis $\mathcal{H}_1$. Otherwise, $\mathcal{H}_0$ is chosen. The value of λ_j is defined a-priori, according to the desired false alarm rate. Notice that if $c_{\max} = 1$, a pure data-fusion CSS takes place.

It is informative to mention that it is not possible to have $c = m_{\mathrm{T}}$ in the proposed hybrid fusion scheme, which would correspond to a pure decision-fusion CSS. In this case, all clusters would have a single SU, preventing PRIDe, or any other SCM-based detector of functioning. In fact, according to the last paragraph of Section 2, the value of c is at most equal to $m_{\mathrm{T}}/2$. Nonetheless, if multi-antenna SUs were considered, a PRIDe test statistic could be formed in all SUs, which would be capable of producing local decision, thus enabling a pure decision-fusion CSS. This multi-antenna approach is not considered in this paper.

3.3. Spectrum sensing performance

The metrics used to assess the spectrum sensing performance are the probability of detection, P_{d}, and the probability of false alarm, P_{fa}. The former is the probability of deciding in favor of an occupied sensed band, given that it is indeed occupied. The latter is the probability of deciding in favor of a vacant band, given that it is occupied. A high P_{d} is desired to protect the primary network against interference of secondary transmission occurring in a band erroneously declared vacant. On the other hand, a low P_{fa} is targeted, aiming at increasing the secondary network throughput.

The performance of the data-fusion CSS in the cluster level, which is measured by the local probabilities of false alarm and detection at the CH of each cluster, cannot be determined theoretically because the probability density functions (PDFs) of the PRIDe test statistic under $\mathcal{H}_0$ and $\mathcal{H}_1$ are unknown [8].

The expressions for calculating the global (at the FC) probabilities of false alarm and detection, in the case of possibly unequal spectrum sensing performance metrics of the SUs in a pure decision-fusion CSS, are given in [35]. These expressions can be adapted to the computation of the global performance metrics of the proposed hybrid fusion scheme, simply replacing the SUs' performance metrics in the original expression of [35] by the CHs' performance metrics, and replacing the number of SUs by the number of CHs. Hence, combining the CHs' decisions under the κ-out-of-c rule at the FC yields the global performance metrics

$$P_{\mathrm{fa}} = \sum_{\ell=\kappa}^{c} \sum_{u=1}^{|\mathbf{D}_\ell|} \prod_{j=1}^{c} {P_{\mathrm{faCH}\,j}}^{D_{\ell_{u,j}}} (1 - P_{\mathrm{faCH}\,j})^{1-D_{\ell_{u,j}}} \tag{12}$$

and

$$P_{\mathrm{d}} = \sum_{\ell=\kappa}^{c} \sum_{u=1}^{|\mathbf{D}_\ell|} \prod_{j=1}^{c} {P_{\mathrm{dCH}\,j}}^{D_{\ell_{u,j}}} (1 - P_{\mathrm{dCH}\,j})^{1-D_{\ell_{u,j}}}, \tag{13}$$

where $|\mathbf{D}_\ell| = \binom{c}{\ell} = \frac{c!}{(c-\ell)!\ell!}$ is the cardinality of the set $\mathbf{D}_\ell$, which is defined as follows: Let $\delta_j = 1$ or $\delta_j = 0$ denote the decision made by the j-th CH in favor of $\mathcal{H}_1$ or $\mathcal{H}_0$, respectively. The set $\mathbf{D}_\ell$ contains the binary c-tuples that satisfy $\sum_{j=1}^{c} \delta_j = \ell$. Thus, $\mathbf{D}_\ell$ can be interpreted as a matrix of order $\binom{c}{\ell} \times c$, and $D_{\ell_{u,j}} \in \{0, 1\}$ is the element sitting on the u-th row and j-th column of this matrix.

In Section 5, the performances of the data-fusion part of the hybrid scheme are measured by means of Monte Carlo simulations and plugged into (12) and (13) for theoretical assessment of the decision-fusion part. Simulations are also made to certify the theoretical performance of this part of the hybrid fusion.

4. Energy consumption model

In this article, a time-division multiplexing (TDM) frame structure is adopted, in which the interval for data transmission is denoted as τ_{t}, and is given by

$$\tau_{\mathrm{t}} = \tau - \tau_{\mathrm{s}} - (m_{\mathrm{T}} - c)\tau_{\mathrm{rSU}} - c\tau_{\mathrm{rCH}}, \tag{14}$$

where τ is the frame duration, τ_{s} is the sensing interval common to the m_{T} SUs, τ_{rSU} is the reporting interval for a single SU to transmit its soft-decision (PU signal samples) to the associated CH, and τ_{rCH} is the report interval for a single CH to transmit its hard-decision to the FC. All intervals are measured in seconds.

The total energy, in joules, spent by the secondary network during a frame can be calculated as

$$E_{\mathrm{T}} = m_{\mathrm{T}}\tau_{\mathrm{s}}P_{\mathrm{s}} + \tau_{\mathrm{rSU}} \sum_{j=1}^{c} \sum_{i=1}^{m_j - 1} P_{\mathrm{txSU}\,i,j} + \tau_{\mathrm{rCH}} \sum_{j=1}^{c} P_{\mathrm{txCH}\,j} + p\tau_{\mathrm{t}} \sum_{j=1}^{c} \sum_{i=1}^{m_j} P_{\mathrm{txDATA}\,i,j}, \tag{15}$$

where P_{s} is the power dissipated by each SU during the spectrum sensing interval; $P_{\mathrm{txSU}\,i,j}$ is the power of the signal transmitted by the ith SU of the jth cluster to the corresponding CH in order to report the PU signal samples associated to the data-fusion part of the hybrid scheme; $P_{\mathrm{txDATA}\,i,j}$ is the power of the signal transmitted by the ith SU of the jth cluster to the FC during the data transmission interval; $P_{\mathrm{txCH}\,j}$ is the power of the signal transmitted by the jth CH to

the FC for reporting the decisions associated to the decision-fusion part of the hybrid scheme; and p is the probability of deciding in favor of a vacant band, which is given by

$$p = p_{\mathcal{H}_0}(1 - P_{\text{fa}}) + p_{\mathcal{H}_1}(1 - P_{\text{d}}), \tag{16}$$

where P_{fa} and P_{d} are the global probabilities of false alarm and detection, and $p_{\mathcal{H}_0}$ and $p_{\mathcal{H}_1}$ are the probabilities of absence and presence of the PU signal in the sensed band, respectively.

Applying the log-distance path-loss model, the values of $P_{\text{txSU}\,i,j}$, $P_{\text{txCH}\,j}$ and $P_{\text{txDATA}\,i,j}$ operated in (15) are respectively computed as

$$P_{\text{txSU}\,i,j} = P_{\text{rxCH}} \left(\frac{d_{\text{CH}_{i,j}}}{d_0} \right)^{\eta}, \tag{17}$$

$$P_{\text{txCH}\,j} = P_{\text{rxFC}} \left(\frac{d_{\text{FC}_j}}{d_0} \right)^{\eta}, \tag{18}$$

and

$$P_{\text{txDATA}\,i,j} = P_{\text{rxFC}} \left(\frac{d_{\text{BS}_{i,j}}}{d_0} \right)^{\eta}, \tag{19}$$

where $d_{\text{CH}_{i,j}}$ and $d_{\text{BS}_{i,j}}$ are the distances from the ith SU of the jth cluster to the jth CH, and to the BS (which is collocated with the FC), respectively, d_{FC_j} is the distance from the jth CH to the FC, and P_{rxCH} and P_{rxFC} are the CHs' and FC' receivers sensitivities (minimum received power levels), respectively. Moreover, recall from (2) that d_0 is the reference distance and η is the path-loss exponent of the log-distance path-loss model.

If no clustering is adopted, that is, if $c_{\max} = 1$, there is a single report interval, τ_{rSU}, for each of the m_{T} SUs to transmit directly to the FC. In this case, (14) specializes to

$$\tau_{\text{t}} = \tau - \tau_{\text{s}} - m_{\text{T}}\tau_{\text{rSU}}, \tag{20}$$

and (15) becomes

$$E_{\text{T}} = m_{\text{T}}\tau_{\text{s}}P_{\text{s}} + (\tau_{\text{rSU}} + p\tau_{\text{t}}) \sum_{i=1}^{m_{\text{T}}} P_{\text{txDATA}\,i,1}, \tag{21}$$

where $P_{\text{txDATA}\,i,1}$ is the power of the signal transmitted by the ith SU to the FC during report and data transmission.

The amount of the successfully transmitted data [36] in the secondary network, measured in bits, depends on the correct identification of a vacant band, and is given by

$$D = p_{\mathcal{H}_0}(1 - P_{\text{fa}})R_{\text{b}}\tau_{\text{t}}, \tag{22}$$

where R_{b} is the data rate in the secondary network, in bit/s. Notice that D/τ_{t} is the secondary network effective throughput, in bit/s.

Finally, aiming at assessing the energy efficiency, the consumed energy per bit [36] of the secondary network, in joule/bit, is computed as

$$E_{\text{B}} = \frac{E_{\text{T}}}{D}. \tag{23}$$

5. Numerical results

This section starts by presenting the pseudo-code associated to the Matlab simulation used to generate the results presented herein. Preliminary numerical results are then provided, aiming at obtaining insights that complement and facilitate the interpretations of the conclusive results subsequently presented.

Pseudo-code associated to the Matlab source code given in [29].

1. Define the values of the system parameters (see Table 1).
2. **For** each randomly-generated cluster set, **Do**:
   2.1) Given m_{T} and $c_{\max}$, perform modified k-means clustering, yielding c and the coordinates of SUs and CHs.
   2.2) Compute $\bar{\sigma}^2$ based on (8) and related equations.
   2.3) **For** the jth cluster of the set, up to $j = c$, **Do**:
      2.3.1) Set m_j according to the number of SUs in the cluster.
      2.3.2) Calculate the distances from SUs to PU, CH, and FC, and from CH to FC.
      2.3.3) **For** each sensing round within a cluster, **Do**:
         2.3.3.1) Plug $\bar{\sigma}^2$ into (3) to get σ_i^2.
         2.3.3.2) Generate PU signal vector $\mathbf{x}$, channel vector $\mathbf{h}_j$, and noise matrix $\mathbf{V}_j$.
         2.3.3.3) Compute $\mathbf{Y}_j$ and $\mathbf{R}_j$ under $\mathcal{H}_0$ and $\mathcal{H}_1$.
         2.3.3.4) Compute $T_{\mathrm{PRIDe}\,j}$ under $\mathcal{H}_0$ and $\mathcal{H}_1$.
         End for (sensing rounds).
      2.3.4) Compute local P_{faCH} and P_{dCH} that form the ROC relative to the jth cluster.
      End for (clusters within a set).
   2.4) Compute the sums of $P_{\mathrm{txSU}\,i,j}$, $P_{\mathrm{txCH}\,j}$ and $P_{\mathrm{txDATA}\,i,j}$.
   2.5) Compute empirical and theoretical global P_{fa} and P_{d}.
   2.6) Compute τ_{t}, P_{d} at the reference P_{fa}, D and E_{T} for the present cluster set.
   End for (cluster set).
3. Compute E_{B} as the average of the quotient between E_{T} (for each of the clusters sets) and D (also for each of the clusters sets).
4. Compute empirical and theoretical global P_{fa} and P_{d} as the average of P_{fa} and P_{d} across the clusters sets.

5.1. Simulation pseudo-code

The pseudo-code shown in the sequel describes the main steps followed by the Matlab simulation code used to generate the results presented in this paper. The associated fully-commented source code is available at [29].

In a few words, the Monte Carlo simulation of the hybrid fusion scheme firstly generates multiple instances of SUs' positions. For each instance, the modified k-means clustering is applied, defining the number of clusters, the cluster members' positions, and the cluster heads' positions. For each cluster, a number of spectrum sensing rounds are executed to yield local probabilities of false alarm and detection. The decisions made at the cluster levels are combined via the κ-out-of-c rule, yielding global probabilities of false alarm and detection. These probabilities, at the clusters and fusion-center levels, are the average of the corresponding metrics attained in all instances of clustering. Theoretical probabilities of false alarm and detection are also computed by the simulation code.

When a parameter is varied to verify its influence on performance and energy consumption, steps 2, 3 and 4 of the pseudo-code are repeated an amount of times equal to the number of parameter values.

In Step 2.5, the theoretical P_{fa} and P_{d} for a given cluster set are computed from (12) and (13), respectively, using the values of P_{faCH} and P_{dCH} read from the receiver operating characteristic (ROC) curve associated to each cluster of the set. In the case of $c_{\max} = 1$, the empirical ROC related to the single cluster becomes the global ROC. As already mentioned, this ROC cannot be found theoretically, since the PDFs of T_{PRIDe} under $\mathcal{H}_0$ and $\mathcal{H}_1$ are unknown. When $c_{\max} > 1$, the empirical P_{fa} and P_{d} in Step 2.5 of the pseudo-code are computed as follows:

1. Firstly, P_{faCH} and P_{dCH} are read from the ROC curve associated to each cluster of a set.
2. For a large number of trials, say 50000, two uniformly-distributed c-tuples $\mathbf{u}_{\mathcal{H}_0}$ and $\mathbf{u}_{\mathcal{H}_1}$ are randomly generated in the interval [0, 1].
3. For each trial, the binary c-tuples $\mathbf{d}_{\mathcal{H}_0}$ and $\mathbf{d}_{\mathcal{H}_1}$ are formed, in which bits 1 represent the condition $\mathbf{u}_{\mathcal{H}_0} < P_{\mathrm{faCH}}$ and $\mathbf{u}_{\mathcal{H}_1} < P_{\mathrm{dCH}}$ (these binary c-tuples represent false alarms and correct detections).

4. Two counters, $C_{\mathcal{H}_0}$ and $C_{\mathcal{H}_1}$ then accumulate, throughout the trials, the events in which the sum of the elements in $\mathbf{d}_{\mathcal{H}_0}$ is greater than, or equal to κ (from the κ-out-of-c rule), and in which the sum of the elements in $\mathbf{d}_{\mathcal{H}_1}$ is greater than, or equal to κ, respectively.
5. The estimated P_{fa} and P_{d} are obtained by dividing $C_{\mathcal{H}_0}$ and $C_{\mathcal{H}_1}$, respectively, by the number of trials.

The procedure just described can be easily identified in the source code [29].

5.2. Preliminary results

Figure 2 shows insightful spectrum sensing performance results, in terms of ROC curves, at the CHs (local) and at the FC (global), for a single random realization of the SUs' positions (shown on the right of each sub-figure) followed by k-means clustering, for $m_{\text{T}} = 15$, $c_{\max} = 1, 3, 5$, SNR $= -12$ dB, $r = 1000$ m, and PU_{tx} location at $(r, r) = (1000, 1000)$ m. The remaining parameters are the default ones listed in Table 1. If necessary, one can retrieve detailed definitions of the parameters from Section 2.

Figure 2a considers $c_{\max} = 1$, i.e. no clustering, yielding a pure data-fusion CSS scheme. The SNR $= -12$ dB has been set to yield $P_{\text{fa}} \approx 0.1$ and $P_{\text{d}} \approx 0.9$. The main objectives of Figure 2a are to serve as reference for Figure 2b and Figure 2c, while demonstrating the exact match between simulation and theoretical results.

In Figure 2b, $c = 3$ clusters resulted by setting $c_{\max} = 3$. This figure shows the ROC associated to each cluster, as well as the simulated and theoretical ROCs at the FC for $\kappa = 1$ (OR), $\kappa = 3$ (MAJ) and $\kappa = 5$ (AND) in the κ-out-of-c combining rule. Again, theoretical and simulated ROCs are in perfect agreement. The particular distribution of SUs yielded quite different local performances, with cluster 3 achieving the best result due to its localization closer to the PU transmitter, even outperforming the global ROCs. The local performance of cluster 2 is poor, owed to its larger distance from the PU transmitter. Notice that cluster 1 outperformed cluster 2, in spite of having 1 SU less, but a closer localization with respect to the PU transmitter. This scenario shows the superiority of the AND rule, followed by MAJ and OR. However, none of these decision-fusion combining rules were capable of providing a global performance superior, or at least equal to the one achieved without clustering (see Figure 2a).

Figure 2c considers $c = 5$ clusters, which resulted from setting $c_{\max} = 5$. Once again, theoretical and simulation results agree. Likewise Figure 2b, the new clustering yielded quite different local performances, and global performances not capable of supplanting the ones given in Figure 2a. Notice that MAJ and AND rules reverse superiority around $(P_{\text{fa}}, P_{\text{d}}) \approx (0.3, 0.7)$, with the OR rule occupying the worst position. In other words, the performance rank among the decision-fusion combining rules is not fixed, as anticipated in Section 1. Observe also an overall performance reduction in comparison with Figure 2b, which is an indication that clustering with progressively larger numbers of clusters tends to yield worse performances. Lastly, notice that the local performances are consistent with the specific SUs' clustering: the best local performance corresponds to cluster 3, which is quite close to the PU transmitter; cluster 5 is even closer, but it has one SU less than cluster 3; the worst local performance refers to cluster 2, which is farther apart from the PU transmitter.

5.3. Conclusive results

This subsection addresses the spectrum sensing performance, measured by means of the global P_{d} for a fixed global $P_{\text{fa}} = 0.1$, and the average energy per bit, E_{B}, consumed by the secondary network, as functions of several system parameters. The simulation results have been generated via the Matlab R2018a, using the source code available in [29]. The default parameters adopted in the simulations are listed in Table 1, unless otherwise explicitly mentioned.

Some of the parameters given in Table 1 need a sort of explanation or justification. The path-loss exponent $\eta = 2.5$ is a typical value in urban environments. The number of samples, $n = 240$, has been determined assuming a channel bandwidth $B = 6$ MHz, sampled at the Nyquist rate during the sensing interval $\tau_{\text{s}} = 20\,\mu$s. A small number of samples has been chosen to contribute with the speed of the simulations; the conclusions obtained with this number apply to any feasible n. Likewise [36], given the frame duration $\tau = 200\,\mu$s, the sensing interval $\tau_{\text{s}} = 20\,\mu$s has been chosen as 10% of τ, and the report interval $\tau_{\text{rCH}} + \tau_{\text{rSU}} = 2\,\mu$s has been chosen as 10% of τ_{s}. Notice that the report interval for decision-fusion, $\tau_{\text{rCH}} = 0.9\,\mu$s, is approximately equal to the one adopted for data-fusion, $\tau_{\text{rSU}} = 1.1\,\mu$s. This is based on [37], where a real frame structure is considered. In such structure, the packet head that is part of the report interval is very large compared to the spectrum sensing data, no matter if this data refers to decisions or digitized samples, meaning that the difference in the report data length for decision-fusion and data-fusion does not bring significant difference to the overall report interval, which becomes approximately the same for both fusion schemes. The mean

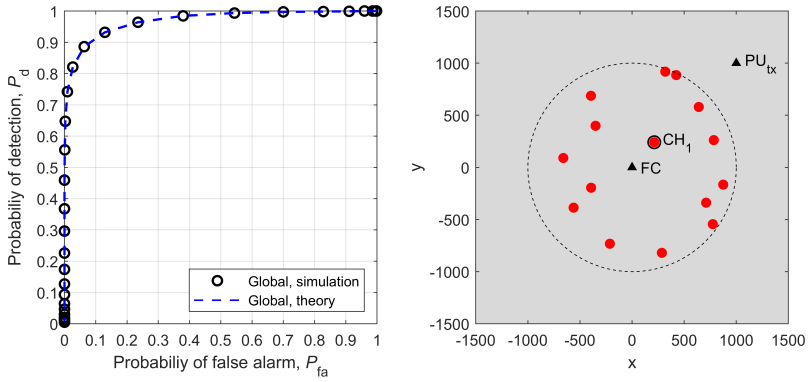

(a)

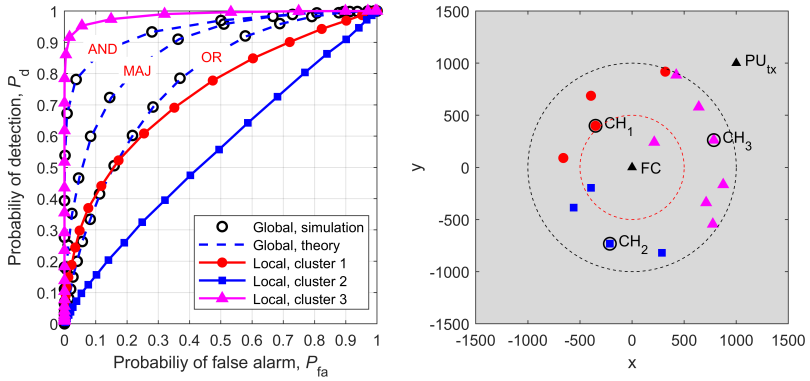

(b)

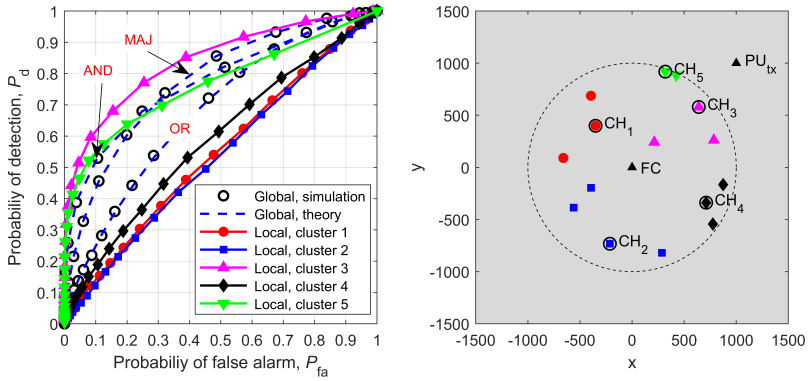

(c)

Figure 2. Local and global ROCs for a realization of the SUs' positions, for $m_T = 15$ and global SNR $= -12$ dB: (a) $c_{max} = 1$. (b) $c_{max} = 3$, cluster SNRs: -12.3, -19.2, -9.3 dB. (c) $c_{max} = 5$, cluster SNRs: -17.9, -20.6, -9.4, -16.3, -8.2 dB. This figure is better viewed in color.

and the standard deviation of the sensing channel Rice factor were defined based on [33], and corresponds to an urban area. The reference $P_{fa} = 0.1$ is in agreement with the IEEE 802.22 standard [6].

Figure 3 shows the global probability of detection, P_d, and the average energy per bit, E_B, versus the maximum number of clusters, c_{max}, for a coverage radius $r = 1000$ m and path-loss exponent $\eta = 2.5$. Figure 3a considers $m_T = 50$, SNR $= -15$ dB, and that the PU$_{tx}$ is located at (r, r) m. Figure 3b assumes $m_T = 30$, SNR $= -14$ dB, and

the PU_{tx} location at $(10r, 10r)$ m. The other parameters are those given in Table 1.

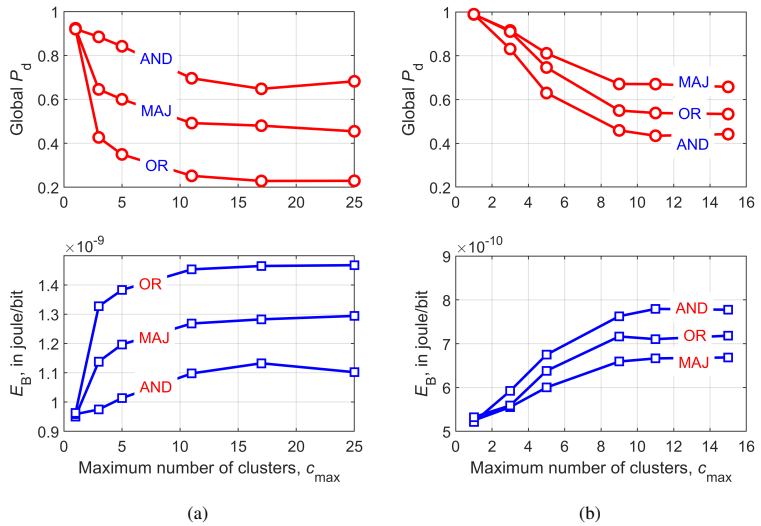

Figure 3. P_d and E_B versus c_{max} for $r = 1000$ m, and $\eta = 2.5$: (a) $m_T = 50$, SNR $= -15$ dB, PU_{tx} at (r, r); (b) $m_T = 30$, SNR $= -14$ dB, PU_{tx} at $(10r, 10r)$.

Figure 3a and Figure 3b unveil an energy consumption inversely-proportional to P_d and directly proportional do c_{max} for any decision-fusion, a result that is supported by the facts:

- The probability p in (15) and (21) has a large influence on E_T, because, for a fixed P_{fa}, a large P_d produces a high p, which in turn yields an smaller E_T.
- From (14), (20) and (22) it can be seen that D does not change too much with the number of clusters, since τ_t changes slightly by changing c, because $\tau_{rSU} \approx \tau_{rCH}$.

Figure 4 illustrates and complements the above-mentioned facts, using the MAJ rule analyzed in Figure 3b as an exemplifying case. It shows the total spent energy, E_T, and the amount of successfully transmitted bits, D, both averaged over all realizations of the cluster sets in the simulation, versus c_{max}, for $r = 1000$ m, $\eta = 2.5$, $m_T = 30$, SNR $= -14$ dB, and PU_{tx} at $(10r, 10r)$. Indeed, a large P_d (see also Figure 3b) yields an smaller E_T, with D changing slightly with c_{max}, and E_T increasing as c_{max} increases. The net result is that E_B increases with the number of clusters.

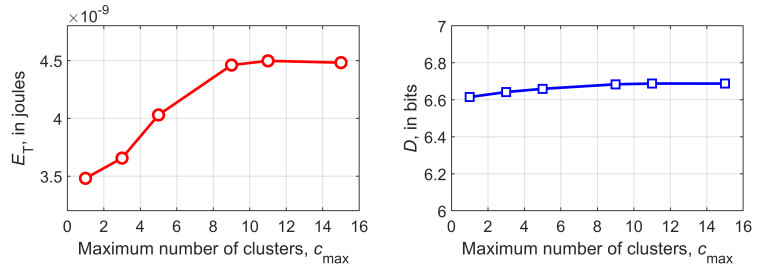

Figure 4. Total spent energy, E_T, and amount of successfully transmitted bits, D, versus c_{max} for the MAJ rule, considering $r = 1000$ m, $\eta = 2.5$, $m_T = 30$, SNR $= -14$ dB, and PU_{tx} at $(10r, 10r)$.

Back to Figure 3, it is an evidence that clustering does not benefit energy savings, meaning that the best option is to adopt a pure data-fusion strategy, which performs better than the hybrid scheme, irrespective to the number of clusters. This strong conclusion, which applies for other values of m_T (results not presented for conciseness), contradicts the common belief that clustering is unconditionally more energy-efficient.

Regarding the comparison among the combining rules, from Figure 3a it can be observed that the AND rule outperforms MAJ and OR in the case of the PU transmitter location at $(r, r) = (1000, 1000)$ m. When this location is changed to (10000, 10000), notice from Figure 3b that the MAJ rule wins, with the OR coming in the second position and the AND rule yielding the worst performance and the largest energy consumption.

Figure 5 highlights the influence of the PU transmitter location on performance and energy consumption, for SNR $= -12$ dB and secondary network coverage radius $r = 1000$ m. Figure 5a considers $c_{\max} = 5$, $m_{\mathrm{T}} = 20$, and $\eta = 1.5$, whereas Figure 5b is for $m_{\mathrm{T}} = 30$, $c_{\max} = 11$, and $\eta = 2.5$. The other system parameters are those listed in Table 1. In both cases, it can be seen exchanges of the performance and energy consumption ranks as the PU transmitter location is modified. When the PU transmitter lies at distances around r or smaller, the AND rule is preferred, with the MAJ occupying the second position and the OR yielding the worst performance and largest energy consumption. The MAJ and AND rules exchange their positions for little larger distances, with the AND rule becoming the worst for even larger distances. For positions beyond $\approx (3r, 3r)$, the MAJ wins in terms of performance, followed by the OR and the AND. The opposite happens in terms of energy consumption. Notice that when the distance between the PU transmitter and the SUs are much larger than the coverage radius of the secondary network, small performance changes are verified if this distance is modified, a consequence of having small differences among the SNRs across the SUs.

From Figs. 2, 3 and 5 it can be concluded that, when the PU transmitter is close to the SUs, the performance of the AND rule improves due to the quite different local performances (caused by quite different SNRs). As the distances from the PU transmitter to the SUs increase, less variation is observed among the local performances, which benefits the MAJ rule. Interestingly enough, the MAJ rule is often mentioned in the literature as being superior to AND and OR. This is because most of the reported analyses assume that the PU transmitter is far enough from the SUs, such that the local performances become approximately the same or, equivalently, the SNRs across the SUs are the same or nearly the same. In such case, it can be seen from Figure 5 that the MAJ rule indeed wins.

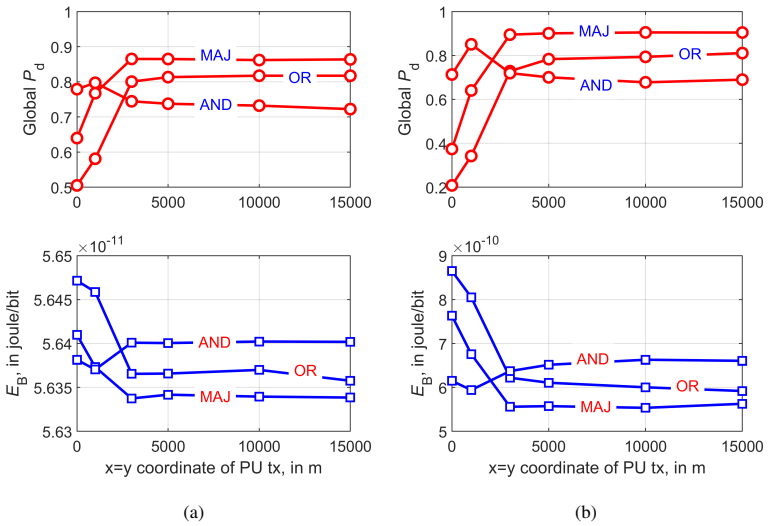

Figure 5. P_{d} and E_{B} versus the location (x, y) of the PU transmitter, for $x = y$, and for SNR $= -12$ dB: (a) $c_{\max} = 5$, $m_{\mathrm{T}} = 20$, $\eta = 1.5$; (b) $m_{\mathrm{T}} = 30$, $c_{\max} = 11$, $\eta = 2.5$.

Figure 6 shows P_{d} and E_{B} versus the path-loss exponent, η, for $m_{\mathrm{T}} = 20$, $c_{\max} = 5$, $r = 1000$ m, and SNR $= -10$ dB. Figure 6a considers that the $\mathrm{PU_{tx}}$ is located at (r, r) m, and Figure 6b assumes that the $\mathrm{PU_{tx}}$ location is $(10r, 10r)$ m. The other parameters are those given in Table 1. When the PU transmitter is close to the SUs, the influence of η on performance is pronounced, except for the AND rule. Notice that the differences between AND, MAJ and OR become larger as η increases. When the PU transmitter is placed farther away from the SUs, η practically does not influence performance. One must be aware that the SNR has been set the same for both locations of the PU transmitter. Thus, it makes sense that the energy consumption grows exponentially with η, since the SUs' transmit powers have been

increased with η to keep the SNR unchanged.

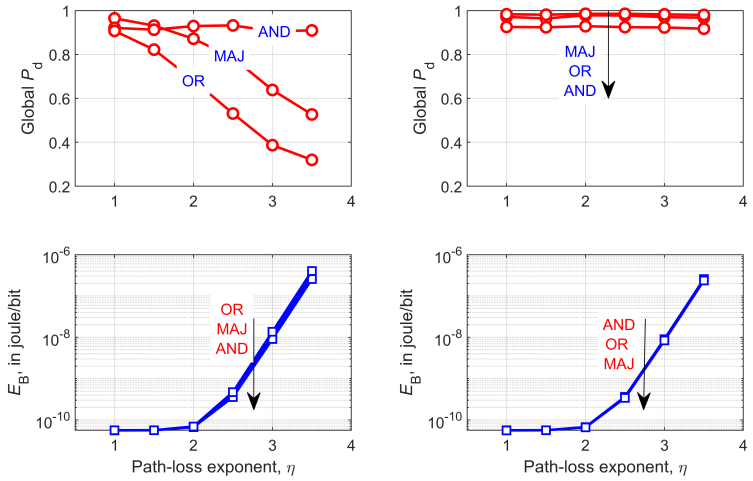

(a) (b)

Figure 6. P_d and E_B versus η for $m_T = 20$, $c_{max} = 5$, $r = 1000$ m, and SNR $= -10$ dB: (a) PU_{tx} at (r, r); (b) PU_{tx} at $(10r, 10r)$.

From Figure 6a it can be also noticed that the MAJ rule is capable of outperforming the AND and OR rules even when the PU transmitter is close to the SUs, but when the path-loss exponent is small. Notably, smaller differences among the local performances occur for large distances from the PU transmitter to the SUs, but also for small distances combined with a small path-loss exponent, since in both cases the SNRs across the SUs become close to each other.

The influence of the total number of SUs, m_T, on performance and E_B is captured by Figure 7. The expected performance improvement as m_T gets large is clearly seen for all decision-fusion rules. Now, the inversely-proportional behavior of E_B with respect to P_d does not appear, since m_T has a stronger influence on increasing E_T than p has on diminishing it, which can be seen from (15). Once again, notice the exchange in the performance rank of the decision-fusion rules, from Figure 7a to Figure 7b, as the result of modifying the PU transmitter location. Notice also that the performance difference among the decision-fusion strategies is smaller for higher distances from the PU transmitter to the SUs, which can be also inferred from Figs. 3, 5 and 6.

6. Conclusions

This paper proposed a hybrid fusion scheme for cluster-based cooperative spectrum sensing, in which the Pietra-Ricci index detector has been used for data-fusion at the cluster heads, combined with decision-fusion of cluster heads' decisions at the fusion center. A modified version of the k-means clustering algorithm has been used to form the clusters, where the cluster heads have been defined as the cluster members closest to the clusters' centroids. Theoretical and computer-simulation results traded the spectrum sensing performance against the energy per bit effectively transmitted during the data communication interval. The results unveiled that cluster-based cooperative spectrum sensing may not benefit energy savings, meaning that the best option is to adopt a pure data-fusion strategy. This is a strong conclusion that contradicts the common belief that clustering is unconditionally more energy-efficient. Moreover, it has been demonstrated that the performance rank of the decision-fusion rules AND, OR and MAJ are strongly affected by the distances between the primary network transmitter and the secondary users, as well as by the path-loss exponent of the channel. The MAJ rule can outperform the others for larger distances or small path-loss exponents, whereas the AND rule is preferred in the opposite situation.

Although the PRIDe has been adopted in the data-fusion part of the proposed hybrid scheme, the conclusions presented herein apply to any other covariance-based detector, since, in principle, a given detector is capable of achieving the same performance of the PRIDe by the proper setting of the system parameters. This is because different models for the sensing channel, for the primary signal or for the noise, as well as different signal power and noise

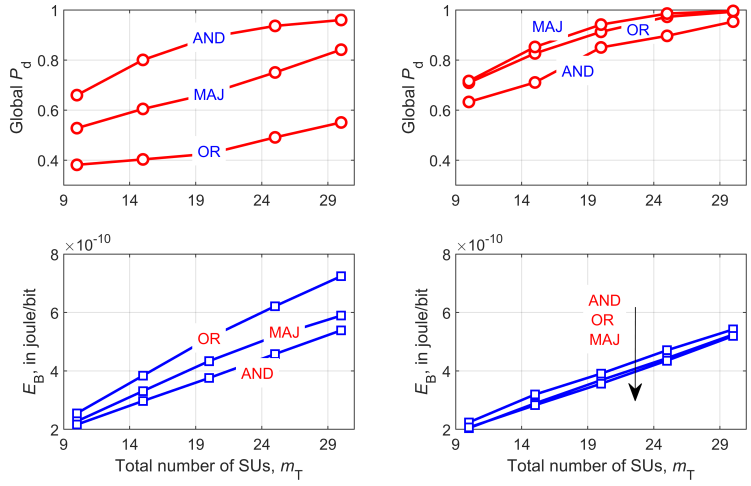

Figure 7. P_d and E_B versus m_T for $c_{max} = 5$, $r = 1000$ m, $\eta = 2.5$, and SNR $= -11$ dB: (a) PU_{tx} at (r, r); (b) PU_{tx} at $(10r, 10r)$.

Table 1. Default system parameters.

Parameter	**Value**
Total number of SUs, m_T	30
Maximum number of clusters, c_{max}	5
Average signal-to-noise ratio over all SUs, SNR	-14 dB
Path-loss exponent, η	2.5
Coverage radius of the secondary BS, r	1000 m
Reference distance for path-loss calculation, d_0	1 m
Number of events for computing the ROCs	500
Number of realizations of cluster sets	200
Secondary network bit rate, R_b	100 kbit/s
Power dissipated per SU during sensing, P_s	1 μW
Number of samples per SU, n	240
Sensing channel bandwidth, B	6 MHz
Frame duration, τ	200 μs
Sensing interval (common to all SUs), τ_s	20 μs
Report interval of each SU to CH or each SU to FC, τ_{rSU}	1.1 μs
Report interval of each CH to FC, τ_{rCH}	0.9 μs
CH receiver sensitivity, P_{rxCH}	-100 dBm
FC receiver sensitivity, P_{rxFC}	-100 dBm
PU transmit power, P_{txPU}	5 W
PU transmitter location, (x, y)	(r, r) m
Fraction of noise power variations about the mean, ρ	0.5
Mean of the Rice factor, μ_K	1.88 dB
Standard deviation of the Rice factor, σ_K	4.13 dB
Probability of presence of the PU signal, $p_{\mathcal{H}_0}$	0.5
Reference P_{fa} for P_d calculation	0.1

levels at the SUs' inputs, or the temporal variation of these quantities, may change both the absolute and the relative performance of a detector, meaning that there exists a particular set of system parameters for which the performance of any of the covariance-based detectors mentioned in Section 1 can be equated to the PRIDe's performance.

The following research opportunities related to the present work can be mentioned: the adoption of imperfect report channels, other clustering algorithms, and more sophisticated path-loss prediction models, as well as the use of realistic node mobility models to assess the dynamics of the energy expenditure, and the addition of correlated shadowing (which may influence the choice of the clustering algorithm), and other test statistics. A weighted hard-decision-fusion at the fusion center can be also addressed. Multi-antenna secondary users, aiming at enabling a pure decision-fusion cooperative spectrum sensing, is also worth investigating.

Acknowledgment

This work was partially supported by RNP (Brazil), with resources from MCTIC (Brazil), Grant 01245.020548/2021-07, under the Brazil 6G project of the Radiocommunication Reference Center (*Centro de Referência em Radiocomunicações* - CRR) of the National Institute of Telecommunications (*Instituto Nacional de Telecomunicações* - Inatel), by Huawei, Grant PPA6001BRA23032110257684, under the project Advanced Academic Education in Telecommunications Networks and Systems, and by CNPq (Brazil), Grant 302589/2021-0.

Appendix A. Expected value of SNR_j

The expected value of SNR_j for $\bar{\sigma}^2 = 1$ can be easily derived by taking into account that the random variables U_i are independent from each other, which allows to write, in light of (4), that

$$\mathbb{E}[\mathrm{SNR}'_j] = \frac{1}{m_j} \sum_{i=1}^{m_j} \mathbb{E}\left[\frac{P_{\mathrm{rxSU}i,j}}{(1+\rho U_i)}\right], \tag{A.1}$$

where the uniform random variable $Z_i = 1 + \rho U_i$ lies in-between $a = 1 - \rho$ and $b = 1 + \rho$.

The expectation of the random variable $P_{\mathrm{rxSU}i,j}/Z_i$ is

$$\mathbb{E}\left[\frac{P_{\mathrm{rxSU}i,j}}{Z_i}\right] = \int_a^b \frac{P_{\mathrm{rxSU}i,j}}{z_i(b-a)} dz_i = \frac{P_{\mathrm{rxSU}i,j}}{b-a} \ln\left(\frac{b}{a}\right). \tag{A.2}$$

Applying this result in (A.1), with $a = 1 - \rho$ and $b = 1 + \rho$, the expected value of SNR'_j for $0 < \rho < 1$ is found to be

$$\mathbb{E}[\mathrm{SNR}'_j] = \ln\left(\frac{1+\rho}{1-\rho}\right) \frac{1}{2\rho m_j} \sum_{i=1}^{m_j} P_{\mathrm{rxSU}i,j}. \tag{A.3}$$

For $\rho = 0$, equation (A.3) yields an indeterminate result that can be easily solved taking into account that

$$\lim_{\rho \to 0} \frac{1}{2\rho} \ln\left(\frac{1+\rho}{1-\rho}\right) = 1,$$

in this case yielding

$$\mathbb{E}[\mathrm{SNR}'_j] = \frac{1}{m_j} \sum_{i=1}^{m_j} P_{\mathrm{rxSU}i,j}. \tag{A.4}$$

References

[1] L. Zhang, M. Xiao, G. Wu, M. Alam, Y. Liang, S. Li, A survey of advanced techniques for spectrum sharing in 5G networks, IEEE Wirel. Commun. 24 (5) (2017) 44–51. doi:10.1109/MWC.2017.1700069.

[2] Y. Arjoune, N. Kaabouch, A comprehensive survey on spectrum sensing in cognitive radio networks: Recent advances, new challenges, and future research directions, Sensors 19 (1).

[3] T. Yucek, H. Arslan, A survey of spectrum sensing algorithms for cognitive radio applications, IEEE Commun. Surveys Tuts. 11 (1) (2009) 116–130. doi:10.1109/SURV.2009.090109.

[4] L. Chen, N. Zhao, Y. Chen, F. R. Yu, G. Wei, Over-the-air computation for cooperative wideband spectrum sensing and performance analysis, IEEE Trans. Veh. Technol. 67 (11) (2018) 10603–10614.

[5] A. Nasser, H. Al Haj Hassan, J. Abou Chaaya, A. Mansour, K.-C. Yao, Spectrum sensing for cognitive radio: Recent advances and future challenge, Sensors 21 (7). doi:10.3390/s21072408.
URL `https://www.mdpi.com/1424-8220/21/7/2408`

[6] The Institute of Electrical and Electronic Engineers, IEEE, IEEE 802 Part 22: Cognitive Wireless RAN Medium Access Control (MAC) and Physical Layer (PHY) Specifications: Policies and Procedures for Operation in the TV Bands (2011).

[7] K. Cichoń, A. Kliks, H. Bogucka, Energy-efficient cooperative spectrum sensing: A survey, IEEE Communications Surveys & Tutorials 18 (3) (2016) 1861–1886. doi:10.1109/COMST.2016.2553178.

[8] D. A. Guimarães, Pietra-Ricci index detector for centralized data fusion cooperative spectrum sensing, IEEE Trans. Veh. Technol. 69 (10) (2020) 12354–12358, doi: 10.1109/TVT.2020.3009440.

[9] L. Huang, Y. Xiao, H. C. So, J. Fang, Accurate performance analysis of Hadamard ratio test for robust spectrum sensing, IEEE Trans. Wirel. Commun. 14 (2) (2015) 750–758. doi:10.1109/TWC.2014.2359223.

[10] R. Zhang, T. J. Lim, Y. C. Liang, Y. Zeng, Multi-antenna based spectrum sensing for cognitive radios: A GLRT approach, IEEE Trans. Commun. 58 (1) (2010) 84–88. doi:10.1109/TCOMM.2010.01.080158.

[11] L. Huang, C. Qian, Y. Xiao, Q. T. Zhang, Performance analysis of volume-based spectrum sensing for cognitive radio, IEEE Trans. Wirel. Commun. 14 (1) (2015) 317–330. doi:10.1109/TWC.2014.2345660.

[12] B. Nadler, F. Penna, R. Garello, Performance of eigenvalue-based signal detectors with known and unknown noise level, in: IEEE Int. Conf. Commun., 2011, pp. 1–5.

[13] D. A. Guimarães, Gini index inspired robust detector for spectrum sensing over Ricean channels, Electronics Letters 55 (12) (2019) 713–714. doi:10.1049/el.2018.7375.

[14] D. A. Guimarães, Robust test statistic for cooperative spectrum sensing based on the Gerschgorin circle theorem, IEEE Access 6 (2018) 2445–2456, doi: 10.1109/ACCESS.2017.2783443.

[15] S. Maleki, S. P. Chepuri, G. Leus, Energy and throughput efficient strategies for cooperative spectrum sensing in cognitive radios, in: IEEE 12th International Workshop on Signal Processing Advances in Wireless Communications, 2011, pp. 71–75. doi:10.1109/SPAWC.2011.5990482.

[16] H. N. Pham, Y. Zhang, P. E. Engelstad, T. Skeie, F. Eliassen, Energy minimization approach for optimal cooperative spectrum sensing in sensor-aided cognitive radio networks, in: The 5th Annual ICST Wireless Internet Conf. (WICON), 2010, pp. 1–9.

[17] S. Althunibat, R. Palacios, F. Granelli, Energy-efficient spectrum sensing in cognitive radio networks by coordinated reduction of the sensing users, in: IEEE Int. Conf. on Commun. (ICC), 2012, pp. 1399–1404. doi:10.1109/ICC.2012.6363804.

[18] J. Lunden, V. Koivunen, A. Huttunen, H. V. Poor, Collaborative cyclostationary spectrum sensing for cognitive radio systems, IEEE Transactions on Signal Processing 57 (11) (2009) 4182–4195. doi:10.1109/TSP.2009.2025152.

[19] S. Appadwedula, V. V. Veeravalli, D. L. Jones, Decentralized detection with censoring sensors, IEEE Transactions on Signal Processing 56 (4) (2008) 1362–1373. doi:10.1109/TSP.2007.909355.

[20] L. D. Nardis, D. Domenicali, M. D. Benedetto, Clustered hybrid energy-aware cooperative spectrum sensing (CHESS), in: T. Kaiser, M. Fidler (Eds.), 4th Int. ICST Conf. on Cognitive Radio Oriented Wireless Networks and Communications, CROWNCOM 2009, Hannover, Germany, June 22-24, 2009, IEEE, 2009, pp. 1–6. doi:10.1109/CROWNCOM.2009.5189147.

[21] F. A. Awin, E. Abdel-Raheem, M. Ahmadi, Designing an optimal energy efficient cluster-based spectrum sensing for cognitive radio networks, IEEE Communications Letters 20 (9) (2016) 1884–1887. doi:10.1109/LCOMM.2016.2585126.

[22] M. A. Hossain, M. Schukat, E. Barrett, Enhancing the spectrum sensing performance of cluster-based cooperative cognitive radio networks via sequential multiple reporting channels, Wirel. Pers. Commun. 116 (3) (2020) 2411–2433. doi:10.1007/s11277-020-07802-4.

[23] H. Ye, J. Jiang, Optimal linear weighted cooperative spectrum sensing for clustered-based cognitive radio networks, EURASIP J. Wirel. Commun. Netw. 2021 (1) (2021) 84. doi:10.1186/s13638-021-01977-5.

[24] Y. Wang, G. Nie, G. Li, C. Shi, Sensing-throughput tradeoff in cluster-based cooperative cognitive radio networks with A TDMA reporting frame structure, Wirel. Pers. Commun. 71 (3) (2013) 1795–1818. doi:10.1007/s11277-012-0911-0.

[25] P. B. Gohain, S. Chaudhari, V. Koivunen, Cooperative energy detection with heterogeneous sensors under noise uncertainty: SNR wall and use of evidence theory, IEEE Trans. on Cognitive Commun. and Netw. 4 (3) (2018) 473–485. doi:10.1109/TCCN.2018.2840134.

[26] S. Althunibat, M. Di Renzo, F. Granelli, Optimizing the K-out-of-N rule for cooperative spectrum sensing in cognitive radio networks, in: IEEE Global Commun. Conf. (GLOBECOM), 2013, pp. 1607–1611. doi:10.1109/GLOCOM.2013.6831303.

[27] E. C. Y. Peh, Y. Liang, Y. L. Guan, Y. Pei, Energy-efficient cooperative spectrum sensing in cognitive radio networks, in: IEEE Global Commun. Conf. (GLOBECOM), 2011, pp. 1–5. doi:10.1109/GLOCOM.2011.6134342.

[28] S. Maleki, S. P. Chepuri, G. Leus, Optimization of hard fusion based spectrum sensing for energy-constrained cognitive radio networks, Physical Communication 9 (2013) 193–198.

[29] D. A. Guimarães, Hybrid fusion of Pietra-Ricci index detector information (6 2023). doi:10.24433/CO.6684888.v1.
URL {https://codeocean.com/capsule/2937729/tree}

[30] S. Lloyd, Least squares quantization in PCM, IEEE Transactions on Information Theory 28 (2) (1982) 129–137. doi:10.1109/TIT.1982.1056489.

[31] T. Kanungo, D. Mount, N. Netanyahu, C. Piatko, R. Silverman, A. Wu, An efficient k-means clustering algorithm: analysis and implementation, IEEE Transactions on Pattern Analysis and Machine Intelligence 24 (7) (2002) 881–892. doi:10.1109/TPAMI.2002.1017616.

[32] The MathWorks, Inc., Matlab *k*-means clustering function help (2021).
URL https://www.mathworks.com/help/stats/kmeans.html

[33] S. Zhu, T. S. Ghazaany, S. M. R. Jones, R. A. Abd-Alhameed, J. M. Noras, T. Van Buren, J. Wilson, T. Suggett, S. Marker, Probability distribution of Rician *K*-factor in urban, suburban and rural areas using real-world captured data, IEEE Trans. Antennas Propag. 62 (7) (2014) 3835–3839. doi:10.1109/TAP.2014.2318072.

[34] D. A. Guimarães, Digital Transmission: A Simulation-Aided Introduction with VisSim/Comm, Springer Verlag, Berlin Heidelberg, Germany, 2009, doi: 10.1007/978-3-642-01359-1.

[35] T. An, D. Kim, I. Song, M. S. Yeu, H.-K. Min, S. Lee, W. Lee, Cooperative spectrum sensing based on generalized likelihood ratio test under impulsive noise circumstances, in: MILCOM 2012 - 2012 IEEE Military Commun. Conf., 2012, pp. 1–6, doi: 10.1109/MILCOM.2012.6415621.

[36] S. Althunibat, F. Granelli, Novel energy-efficient reporting scheme for spectrum sensing results in cognitive radio, in: IEEE Int. Conf. on Commun. (ICC), 2013, pp. 2438–2442. doi:10.1109/ICC.2013.6654897.

[37] L. Zhu, C. Yao, L. Wang, The optimization of combination scheme in cooperative spectrum sensing based on the practical reporting frame format, Wirel. Pers. Commun. 102 (4) (2018) 3009?3019. doi:10.1007/s11277-018-5322-4.
URL https://doi.org/10.1007/s11277-018-5322-4